

Document downloaded from:

<http://hdl.handle.net/10251/181396>

This paper must be cited as:

Khorami, M.; Navarro-Gregori, J.; Serna Ros, P. (2021). Serviceability behaviour of reinforced UHPFRC tensile elements: Assessment of the ratio between maximum and average crack widths. *Construction and Building Materials*. 303:1-14.
<https://doi.org/10.1016/j.conbuildmat.2021.124513>



The final publication is available at

<https://doi.org/10.1016/j.conbuildmat.2021.124513>

Copyright Elsevier

Additional Information

Serviceability behaviour of reinforced UHPFRC tensile elements: Assessment of the ratio between maximum and average crack widths

M. Khorami^{1,2}, Juan Navarro-Gregori^{*1}, and P. Serna¹

1: Institute of Science and Concrete Technology, ICITECH, Universitat Politècnica de València,
València, 46022, Spain.

2: Universidad UTE, Facultad de Arquitectura y Urbanismo, Calle Rumipamba s/n y Bourgeois, Quito, Ecuador

Corresponding Author: Juan Navarro-Gregori, Associate Prof., Universitat Politècnica de València, Spain.

Email address: juanagre@cts.upv.es Tel: +34-963877007-75617

Orcid: Khorami 0000-0003-4592-0233; Navarro-Gregori 0000-0002-6319-7029; Serna 0000-0001-8754-1165

Abstract

This study aimed to evaluate the maximum crack width formed under tensile stresses for two reinforced ultra-high performance fibre-reinforced concrete (UHPFRC) types with different steel fibre volume contents, and to compare them to average values. The maximum crack width values can more than double the average ones based on the applied tensile strain. The difference between maximum and average crack widths should be considered for examining UHPFRC structures for the serviceability and durability design. This paper also introduces appropriate statistical procedures for developing fragility curves based on cracking data by assuming that they can be represented by Rice distribution functions.

Keywords: Serviceability behaviour; tensile elements; UHPFRC; cracking behaviour; durability, fragility curve.

1. Introduction

The durability of reinforced concrete structures to environmental actions is essentially related to controlling crack width under specific environmental conditions, while preventing steel corrosion caused by increasing chloride ions and carbon dioxide.

Concrete cracking degrades required performance, such as safety and serviceability, due to steel corrosion during the design working life. Cracking examinations can be done by controlling the crack width of concrete structure elements to meet the crack width limitations to avoid steel corrosion as determined under specific environmental conditions. Another

parameter to examine cracking is predicting the chloride ion concentration upon steel reinforcement under specified environmental conditions, while limiting it to the permissible concentration for steel corrosion onset during working life. Both concrete cover and concrete quality are other parameters applied to verify if steel is protected from corrosion due to chloride ion ingress. Water tightness and structure appearance are important factors for examining cracking and permissible crack width, and should be specified for such cases. Controlling crack width in UHPFRC is essential for resisting environmental actions, serviceability behaviour and safety, and for avoiding steel corrosion and aesthetics during UHPFRC structures' working life. To design UHPFRC structural elements, resistance to environmental actions should be examined by controlling crack width, while cracks should be tested (due to stresses) to control impaired structures' serviceability and safety [1, 2]. The capability of controlling crack width is the major characteristic of UHPFRC structural members [3-6]. The characteristic crack width (considered as a cautious estimate of the true value of crack width such that there is a probability of 95% the mean value is lower than the calculated) should be calculated by applying an appropriate combination of actions [7-10]. On predicting crack width in the literature, Borosnyói and Balász [11] summarized different approaches as four categories:

- (a) An analytical approach for calculating crack width by solving the differential equation of bond-slip
- (b) A semi-analytical approach for calculating the average crack width (w_m) as the product of the mean crack spacing (s_{rm}), and the difference between the mean strain in the reinforcement (ε_{sm}) and the mean strain in the concrete between cracks (ε_{cm})

In this case, the characteristic crack width (w_k) value can be calculated by the following relation:

$$w_k = \beta \cdot w_m = \beta \cdot s_{rm} \cdot (\varepsilon_{sm} - \varepsilon_{cm}) \quad (1)$$

where (β) is a factor that relates the average crack width to the characteristic value.

According to different authors and design codes, β factor is supposed to lie between 1.3 and 2 [12-16]. For example, the Spanish design code for concrete structures (EHE-08) [15] recommends β equalling 1.3 if cracking is caused by indirect actions only, and 1.7 otherwise. It should be noted that current concrete design codes, such as CEB-FIP Model code 2010 [7], Eurocode 2 [8], and French code NF P 18-710 for UHPFRC structures [17], do not explicitly use β for calculating crack widths, but the characteristic crack width is calculated directly by

multiplying the crack spacing $s_{r,max}$ by the difference in the longitudinal reinforcement and concrete mean strains ($\varepsilon_{sm} - \varepsilon_{cm}$):

$$w_k = s_{r,max} \cdot (\varepsilon_{sm} - \varepsilon_{cm}) \quad (2)$$

Borosnyói and Balász [11] calculated the characteristic average crack width ratio ($\beta = w_k / w_m$) by using the formula recommended by MC90 [18] for a rectangular concrete cross-section with a reinforcement ratio of 0.5% to 2.5%, and a concrete compressive strength from 30 to 50 N/mm². They demonstrated that $\beta = 1.5$ and is independent of both the reinforcement ratio and concrete strength.

- (c) An empirical relation based on fitting a large number of experimental data
- (d) A numerical model, such as FEM models, fracture mechanics models or damage models.

If steel fibres are used in concrete, such as fibre-reinforced concrete (FRC), the crack width calculation is similar to that of normal reinforcement concrete, and the general equation for determining the characteristic crack width value can be used (Eq. 2), while the tensile stress in FRC not equalling zero after cracking should also be considered [7]. According to RILEM TC 162-TDF 2003 [19], crack width is calculated by Eq. 1 when considering factor β to be 1.7 for load-induced cracking and 1.3 for restrained cracking in those sections with a minimum depth of 300 mm or less. With UHPFRC elements, E. Fehling et al [20] indicated that the characteristic crack width value can be determined by the general equation for crack width calculations (Eq. 2), and proposed an expression for calculating the mean strain difference between bar reinforcement and the concrete between cracks [21-25].

In order to investigate reinforced concrete's cracking behaviour, the uniaxial tensile test is normally performed and prismatic concrete specimens are used with steel reinforcement in the central section. Following the literature [26-30], the average measured crack width on the surface can be obtained by dividing the total tensile elongation by the number of cracks. An experimental study was carried out that involved testing a dog bone-shaped UHPFRC tie element to find the relation between the maximum experimental measured crack width with the average crack width.

2. Research significance

Controlling crack width is a fundamental parameter to design reinforced UHPFRC (R-UHPFRC) structures under serviceability conditions. As tensile microcracks occur along

specimen length, and obtaining the crack width for each crack in each force stage is often complicated, the average crack width is considered to be an empirical output and the solution is computed as follows:

$$\text{Average crack width} = \frac{\text{Extended recorded length during test}}{\text{Number of cracks}}$$

The existing difference between the maximum measured crack width and the average value should be considered for examining R-UHPFRC structures for the serviceability limit state (SLS), and for their durability. Test results provide valuable information about the SLS for developing further design recommendations for R-UHPFRC members.

3. Serviceability design and conditions

The SLS requirements are applied to concrete reinforcement structures to guarantee their functionality and structure integrity under service conditions. To verify the SLS and to define the serviceability requirements for concrete structures, the SLS is normally considered by restraining stresses in material, crack width and spacing restriction, structure element vibration, and long- or short-term deflections. The stress level (tension and compression) should be controlled under service loads in both concrete and steel reinforcement. Under SLS loads, compression stresses are normally limited by design codes to avoid excessive compression stresses, longitudinal cracks and excessive creep deformations. The French code NF P 18-710 [17] requirements for UHPFRC elements resemble the RC and FRC elements provided by Eurocode 2 [7], and limit compressive stress with a value of $0.6 f_{ck}$ (compressive concrete strength). Japanese UHPFRC design recommendations [31] limit compressive stresses to $0.4 \cdot f_{ck}$ under permanent loads. If tensile stresses are limited in reinforcement, an appropriate safety margin needs to be set below the yielding strength to prevent uncontrolled cracking [7]. Under serviceability conditions, inelastic reinforcement deformation should be avoided to prevent large and permanently open cracks. For RC and FRC structural elements, Model Code 2010 [7] indicates that tensile rebar stress does not exceed $0.8 \cdot f_{yk}$ (the characteristic tensile yield stress value of reinforcement) and French code NF P 18-710 [17] applies the same tensile stress limitation requirement for UHPFRC elements. Japanese UHPFRC design recommendations [31] indicate that steel reinforcement behaviour should be elastic under compression and perfectly elastoplastic under tension. Steel tensile stress is also limited to the characteristic steel tensile strength value (f_{yk}).

Concrete stress verification in the SLS for UHPFRC depends on the post-cracking behaviour under uniaxial tensile stresses (strain-hardening or strain-softening behaviour). French code NF P 18-710 [17] categorizes tensile UHPFRC behaviour as three classes: T1 (tension-softening), T2 (slight strain-hardening) and T3 (considerable strain-hardening). According to this code, cracking control is not necessary for UHPFRC class T3, but for classes T1 and T2 provide a crack opening expression. It is worth mentioning that Swiss standard fprSIA 2052 [27] verifies SLS requirements by limiting the maximum tensile concrete stress up to 90% of the characteristic elastic tensile strength value for UHPFRC with strain-hardening tensile behaviour, and up to 70% for UHPFRC with tension-softening behaviour. As a plural and identical agreement for serviceability requirement and an SLS design is lacking for R-UHPFRC, further research is necessary.

4. Experimental Program

In this study, an experimental test was run to specify and evaluate the maximum and average crack widths for R-UHPFRC tensile elements. Eight dog bone-shaped concrete specimens with two different UHPFRCs in distinct fibre content terms were manufactured. Four specimens with UHPFRC by a 2 vol.% fibre content, and four specimens with UHPFRC by 1 vol.%, were cast.

All eight series of dog bone-shaped elements were produced, and their size and reinforcement rebar diameter were the same to ensure identical geometrical conditions. In this circumstance, the presence of two different fibre volume contents for specimens is capable of evaluating the fibre content influence on cracking behaviour and crack width values under tensile force.

4.1. Test setup

The equipment to be used to carry out tests was designed to perform the direct tensile test using R-UHPFRC specimens with the dog bone-shaped geometry. The main test setup part included a steel frame with four longitudinal steel tube sections ($60 \times 60 \times 6$ mm) and two steel plates ($320 \times 320 \times 50$ mm) at both ends. A hydraulic jack was installed at one end of the steel frame to apply tensile force to the reinforcement placed into the concrete specimen. Two measurement systems were employed for measuring the applied force: the first for measuring the pressure of oil in the hydraulic jack, and another used the cell-force measurement equipment. This cell-force equipment was installed alongside the endplate on the other steel frame side (see Fig. 5). The connection between the R-UHPFRC specimen and the transformer force system included two steel (2 mm-high) jaw-indented corrugations assembled by six bolts.

The main steel test frame, the hydraulic jack, the installed specimen and the jaw details are shown in Figure 1.

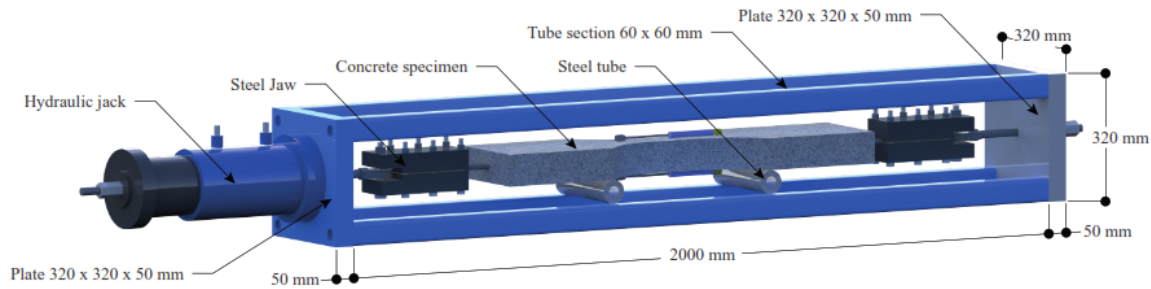


Figure 1. Test setup detail

Tensile force was transferred to the concrete specimen by the friction between jaws and reinforcements. The authors have published the complete details of the test setup system, and the process of performing direct tensile tests, to study R-UHPFRC prismatic tensile elements under serviceability loads [28].

4.2. Specimens and material

4.2.1. Preparing dog bone-shaped specimens

All the dog bone-shaped UHPFRC ties were reinforced with a steel rebar ($\text{Ø}12$ mm) in such a way that the rebar passed from the central cross-section of the tie and lay along it. According to the jaw geometry, to connect the specimen to transfer force system, and to avoid yielding rebar failure outside the specimen at two ends, it was necessary to attach two additional rebars at the two main rebar ends. These rebars were welded on its end to the main rebar by 5-cm welding. The general geometry of the dog bone-shaped specimens, the reinforcement details and the wooden mould geometry are shown in Figure 2.



Figure2. Dog bone-shaped specimen and reinforcement detail

The dog bone shape was used for tensile elements to prevent cracking at the specimen end zone (end-effect), specifically where there is a stiffness difference between the section with the three steel rebars and the section with one steel rebar (see Fig. 2: Sections 1 and 2). Based on the experience acquired by the authors in previous works and from running lots of direct tensile tests of prismatic R-UHPFRC tensile elements [28, 29], the dog bone-shaped specimen was herein suggested to increase the stiffness of the ties in the end zones to prevent any undesired crack occurring beyond the studied zone. Another reason for using the dog bone shape was to obtain a small limited zone over the specimen to measure crack widths by a microscope camera. This small zone is essential because detecting all the cracks along the entire tie element length is time-consuming. Dog bone specimens are generally used for specifying the mechanical tensile properties of small-sized fibre-reinforced concretes with no reinforcement bars. Some codes and recommendations provide standard dimensions for performing direct tensile tests for dog bone-shaped concrete or mortar specimens, such as the Japanese recommendation [26], the Swiss standard [27], ASTM C190-85 [32] and JSCE [33]. In this study, the dog bone-shaped specimens were designed as so: 1050 mm long, 240 mm wide, and 80 mm at both ends and at the middle of elements, respectively. Thickness was 80 mm and remained constant along the specimen (Fig. 3).

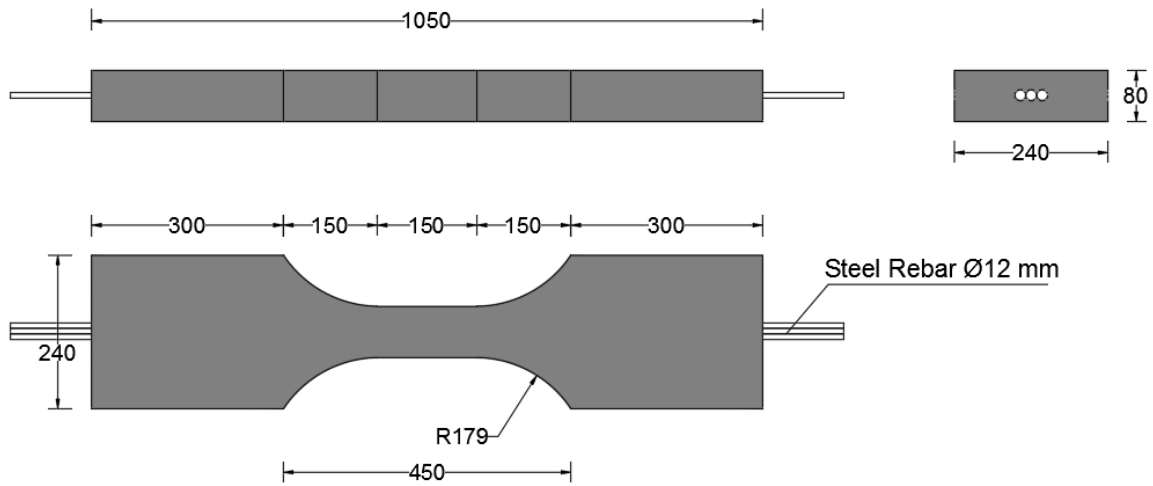


Figure 3. Specimen geometry and dimensions (units: mm)

The central specimen zone (length $L=150$ mm) had a constant width, and the cross-section at the centre of the tie was 80×80 mm² with a reinforcement ratio of $\rho = 1.76\%$. During the test, almost all the tensile cracks took place in this zone, and no crack occurred at the section from the changing stiffness. To facilitate the microscope camera's movements over lateral specimen surfaces, a semihard plastic laminate was glued to the mould surface at the specimen mid-part to create a smooth surface on the lateral UHPFRC surfaces. This created smooth surface helped to improve image resolution, and to better visualize the crack width on the UHPFRC specimen surface.

4.2.2. Mix design

UHPFRC is composed of cement, water, aggregates, additives, admixtures and fibres. The difference between UHPFRC and conventional concrete mix designs lies in the amount of binder, aggregate sizes and the presence of fibres. To accomplish acceptable UHPFRC workability, it is necessary to use superplasticizers (SP). UHPFRC is generally much denser and it is important to achieve the maximum possible packing density to improve mechanical and durability properties. The mix design herein employed aligns with previous works performed by the authors [28, 29, 34]. Two UHPFRC types were developed with different fibre contents for this experimental study. The UHPFRC-type one (U1) included 2 vol.% of steel fibres, which is the equivalent to 160 kg/m³ of steel fibre content. The second UHPFRC type (U2) contained 1 vol.% (80 kg/m³). Small-sized steel fibres were used in UHPFRC as so: 13 mm long, a diameter of 0.2 mm and tensile strength beyond 2000 MPa. The nominal yield stress of rebars was 500 MPa. The composition of the UHPFRC mixtures is given in Figure 4.

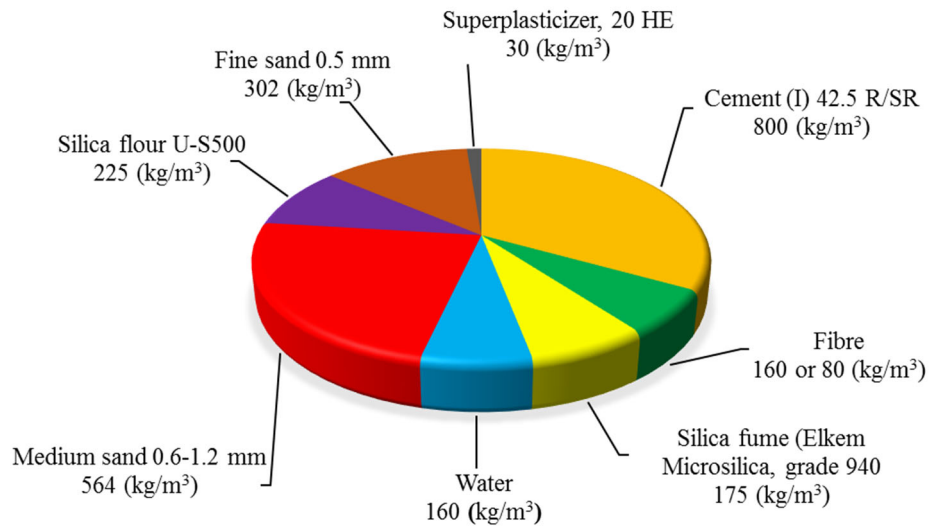


Figure 4. The proportion of UHPFRC components [28, 34]

The UHPFRC mixture must achieve good workability, particle distribution and packing density by the end of the mixing process. As it contained constituents and fine particles, and given its tendency to agglomerate, breaking these chunks would be easier if particles were dry. Hence mixing all the fine dry particles before adding water is recommended [35, 36]. The mix procedure started by placing all the dry aggregates and mixing them for 1 minute. Then water and the additive were gradually added. Mixing continued for 5 minutes to make it completely workable. Small steel fibres were gradually added to the flowable mixture. UHPFRC was mixed for another 5 min. to avoid the chunks formation of fibres in concrete. The complete mixing time was 16 min., which was done in a standard horizontal 100-liter mixture machine. As the tensile response of the UHPFRC is affected by fibre distribution and orientation, a specific casting and specimen production process was followed to ensure the same fibre distribution and orientation in all specimens. The UHPFRC was always placed slowly into the moulds from one end and allowed to flow through the entire tensile element. The influence of other pouring procedure or specimen's geometry on the crack pattern is out of the scope of this work. In this study, four specimens were cast per concrete type and one UHPFRC batch was prepared for every two specimens. Compressive UHPFRC strength was measured on four cube samples (100 mm in size). The average compressive strength for each batch and the corresponding specimen code are found in Table 1.

Batch number /UHPFRC type	Specimen code	Compressive strength of each cube sample (MPa)	Average value (MPa)
Batch #1/ U1-160	DB #U1-1 & DB #U1-2	171.7	161.8 (CV=7.0%)
		158.3	
		147.3	
		169.8	
Batch #2/ U1-160	DB #U1-3 & DB #U1-4	163.5	158.4 (CV=6.6%)
		145.0	
		169.3	
		155.9	
Batch #1/ U2-80	DB #U2-1 & DB #U2-2	157.1	157.6 (CV=3.5%)
		164.6	
		157.3	
		151.2	
Batch #2/ U2-80	DB #U2-3 & DB #U2-4	148,0	156.0 (CV=1.7%)
		153.4	
		158.7	
		155.8	

Table 1. The average compressive strength value of each UHPFRC batch and the specimen nomenclature

The average compressive strength values for both UHPFRC types (4 batches) were similar. The coefficient of variation (CV) values were low, which means that the UHPFRC matrix for all the batches was almost the same (with 5% CV for all the compressive results for both UHPFRC types) and fibre content did not significantly influence UHPFRC compressive strength.

Other important mechanical UHPFRC properties are tensile strength and postcracking behaviour. These tensile properties can be obtained from the load-deflection curve following an inverse analysis method. Although ideal UHPFRC is deemed to show strain hardening behaviour in tension, some standards such as NF P 18-710 [17] accept UHPFRC with low strain softening behaviour. In this paper an inverse analysis method proposed in [37, 38], adapted to UHPFRC with strain-softening behaviour [39] was applied to characterize the tensile properties ($\sigma - \varepsilon$ constitutive law) of the UHPFRCs used (see Table 2) [34]. This behaviour is related with the low dose of steel fibres used to produce economically competitive UHPFRCs [40].

Constitutive Relation Model Parameters (average result value)	f_t (MPa)	$\varepsilon_{t,el}$ (‰)	$f_{t,u}$ (MPa)	$\varepsilon_{t,u}$ (‰)
U1 ($V_f=160 \text{ kg/m}^3$)	9.41	0.18	8.49	6.56
U2 ($V_f=80 \text{ kg/m}^3$)	6.41	0.13	5.81	1.98

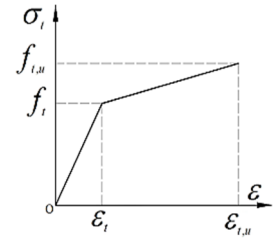


Table 2. Tensile properties of concrete types U1 and U2 [34].

The purpose of using UHPFRC with a low dose of microsteel fibres was to gain economical concrete that acceptably performs in the SLS.

4.3. Test procedure

The dog bone-shaped R-UHPFRC specimens were horizontally placed inside the test frame machine. The R-UHPFRC specimen was connected to the force transfer system by two steel jaws at each end by placing it inside the jaw and fixing it by tightening six bolts. The horizontal specimen position in the test frame system conferred good access and facilitated the microscope camera's movements over the lateral specimen surfaces during the direct tensile test. To reduce the specimen's self-weight effect and the resulting bending in the middle of the specimen, two steel tubes were placed under the specimen on each one-third of the length from the ends as roller supports (see Fig. 5).

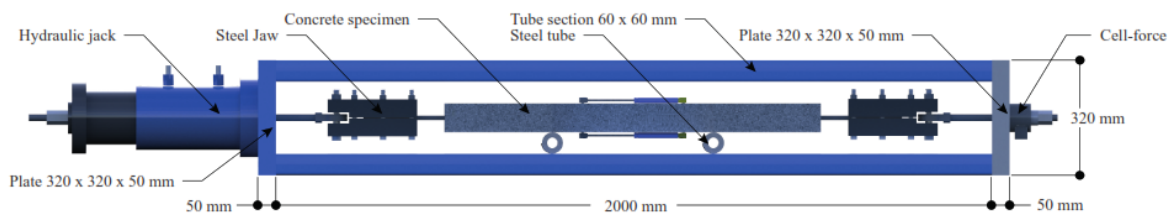


Figure 5. Placing the specimen inside the steel frame and roller support

In order to measure R-UPFRC specimen elongation, particularly in the study area (central testing zone), two displacement transducers (DTs) were installed on the up and bottom specimen surfaces (300 mm length). Before the main tests were run, one specimen was tested as a prototype sample to evaluate both the accuracy and efficiency of the measurement process. As some cracks occurred outside the test zone, a decision was made for measurements to be taken on a longer length. The DT length of 300 mm was chosen for this purpose. A simple linear finite element model of the dog-bone specimen was made to evaluate the difference

between the deformation measured in the central testing zone and the DT length of 300 mm. The deformation measured over the central testing zone was about 8% greater than the DT length zone, which would not significantly affect the results.

The applied force was measured by the load cell equipment. The load-displacement behaviour curve of the R-UHPFRC specimens was also recorded by considering the data obtained from both DTs and the load cell. Crack monitoring and detecting crack widths during the test were performed on the lateral R-UHPFRC surface on the specimen's mid-part where the tensile element had a square section ($80 \times 80 \text{ mm}^2$). Cracks were detected by a microscope camera at three specimen thickness levels: bottom, middle and top. The first line passed the specimen's longitudinal axial elevation, which corresponded exactly to the rebar axis. The second and third lines were located at a 10-mm distance from the top and bottom lateral surface edges (Fig. 6). These lines were marked on the surface with a pen to move the microscope camera on the direct line over these lines, which were divided into three different colours to denote millimetre divisions. The central testing zone and the guiding lines on the specimen's lateral surface are shown in Figure 6.

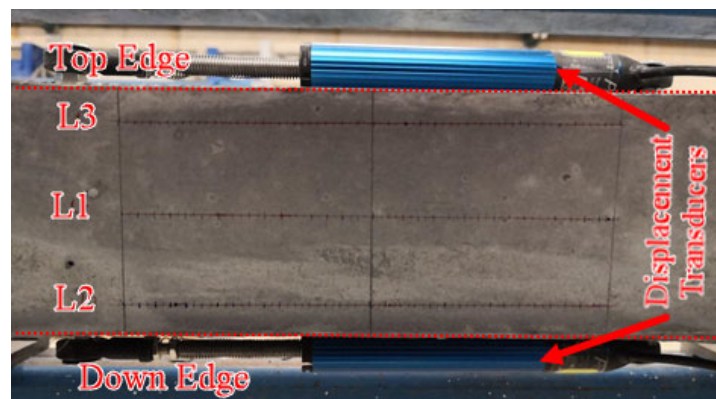


Figure 6. The three guiding lines for detecting cracks on the lateral surface

The intention of measuring crack width at the three different elevation levels (bottom, middle, top) was to better observe the formed inhomogeneous crack propagation. Moreover, given the possibility of the width of the tensile cracks along the length (perpendicular to the longitudinal applied force) not being constant, the width of the formed cracks could be wider on the edges or in the middle over the reinforcement axis. Figure 7 illustrates the cracking possibilities of the tie element and the different crack forms. This could be due to the existing bending caused by either the specimen's self-weight or improper reinforcement rebar placing. One suggestion was to take crack width measurements over the three lines located on the bottom, middle, top

elevations of specimen thickness to obtain clear crack properties. Section 5.1 describes the crack width calculation.

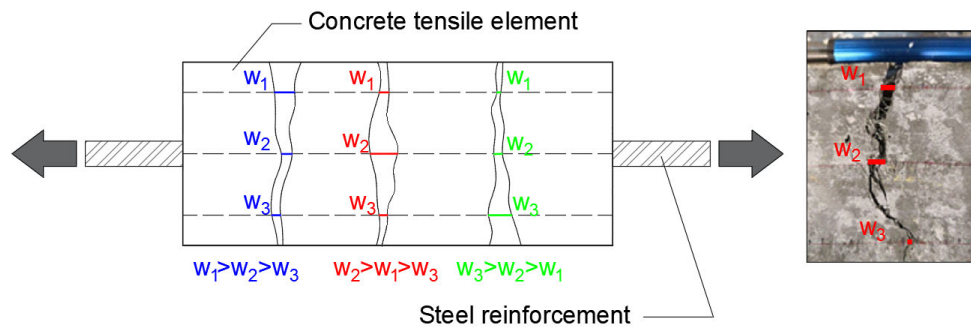


Figure 7. The crack formation and crack width variation possibilities along its length

The tensile test began by applying tensile elongation to the R-UHPFRC specimen. The video recording of the specimen's surface was done at the different applied tensile elongation levels (almost by increasing 0.5‰ for each level) and the force value was recorded at these levels.

4.4. Crack width measurement

When the video recording of the surface over each line began, the concrete crack width ruler card was placed on the specimen surface and acted as a base for the measurement taken to calculate crack width. Then the recorded video was analysed and reviewed on the desktop monitor. By making a linear proportional calculation between the marked line on the crack width ruler card and the crack mouth opening on the monitor, the real crack width was calculated. As the video recording over lines was time-consuming, both the applied force value and tensile elongation could slightly change. When video recording started and ended (with an average duration of 3 minutes for each strain level and each line), the applied force value and tensile elongation were noted, and the average mean value was used for the subsequent analysis. In this experimental work, an attempt was made to detect the first formed crack. To this end, the first microscope camera video recording of the surface was taken at very low tensile strains (0.03‰ to 0.05‰). As previously mentioned, the average crack width can be obtained by dividing tensile elongation by the number of cracks. To do so, the number of cracks that formed on each line was counted in each stage. The crack width measurement was taken for a minimum of 10 tensile strain levels. With the obtained experimental data, it was possible to draw both the force-elongation and crack width-elongation at the same time and on the same graph. These obtained results and diagrams are herein found in Section 5. The objective of this study was to evaluate both the cracking and tensile behaviours of the R-UHPFRC tie up to the 2.0‰ tensile strain level. However, the tensile test was performed for a higher tensile strain

and, therefore, two additional crack width recordings were taken at the 2.5‰ and 3.0‰ strain levels.

5. Test results and discussion

5.1. Average crack width

Attempts were made to measure the crack width for all the specimens at the same tensile strain level. Due to cracking, the applied elongation sometimes increased suddenly and could not be controlled. As incremented elongation was not generally marked, it had no significant effect on the presented results and diagrams. By way of example, the detailed test data and results obtained from specimen DB #U1-1 are explained below. To present the behaviour of the R-UHPFRC specimen under the applied average tensile strain, a diagram was used so that the top side of this diagram would show the force-strain relation and the downside would depict the crack width-strain. The first video recording was done at a very low tensile strain (0.03‰) to detect the possible precreated cracks due to shrinkage. The video recording process started on the specimen surface from the centre line (L1). Table 3 provides the average tensile strain and tensile force at the start and end of the video recording on every line and for each average strain level for specimen DB #U1-1.

For this specific specimen (DB #U1-1), no cracks were observed up to the tensile strain of 0.10 ‰, and the first cracks were detected at the fifth level of the applied average tensile strain with a value of 0.291‰ at the level force value of 42.8 kN (see Table 3). The number of cracks increased clearly with rising the applied average tensile strain (see the number of cracks column in Table 3). The force-strain relation and the average crack width-strain relation of specimen DB #U1-1 are presented in Fig. 8. The presented average crack width is based on the number of cracks detected on the central line (L2) exactly over the rebar axis.

# Strain level	# Line on the surface	Initial Force (kN)	Initial Avg. Strain (‰)	Number of cracks	Final Force Value (kN)	Final Avg. Strain (‰)
N1	L3	18.1	0.0296	0	17.3	0.0296
	L2	18.1	0.0296	0	17.7	0.0311
	L1	18.0	0.0311	0	17.6	0.0311
N2	L3	25.2	0.0552	0	24.4	0.0566
	L2	25.0	0.0566	0	23.9	0.0551
	L1	25.8	0.0581	0	24.5	0.0581
N3	L3	33.3	0.0808	0	31.8	0.0793
	L2	31.8	0.0808	0	30.5	0.0808
	L1	31.7	0.0808	0	30.4	0.0808
N4	L3	37.0	0.1390	0	35.4	0.1390
	L2	35.6	0.1420	0	35.5	0.1420
	L1	36.4	0.1420	0	35.0	0.1420
N5	L3	45.1	0.2140	0	42.7	0.2930

	L2	42.8	0.2910	4	40.2	0.2910
	L1	43.2	0.2940	4	40.6	0.2960
N6	L3	51.2	0.5170	0	47.6	0.6500
	L2	47.0	0.6510	6	46.9	0.6510
	L1	47.6	0.6510	9	44.0	0.6480
N7	L3	56.1	0.8140	1	52.5	0.8410
	L2	55.2	0.8510	8	51.7	0.8680
	L1	54.8	0.8800	11	51.8	0.8790
N8	L3	61.2	1.1600	2	58.1	1.1500
	L2	62.1	1.1100	10	58.5	1.1200
	L1	61.1	1.1300	13	58.0	1.1400
N9	L3	68.9	1.4200	3	64.7	1.4300
	L2	64.2	1.4300	13	63.7	1.4300
	L1	65.2	1.4400	15	62.5	1.4300
N10	L3	81.4	2.0200	11	76.9	2.0200
	L2	80.8	2.0400	19	76.8	2.0300
	L1	80.1	2.0300	18	76.4	2.0300
N11	L3	92.2	2.5200	14	87.0	2.5300
	L2	90.2	2.5500	21	85.6	2.5300
	L1	90.3	2.5400	17	85.9	2.5400
N12	L3	99.8	3.1000	17	93.8	3.0700
	L2	93.0	3.1000	23	93.4	3.0700
	L1	92.2	3.1000	19	92.8	3.0700
N13	L3	-	-	-	-	-
	L2	10.1	4.6000	25	93.1	4.5200
	L1	-	-	-	-	-

Table 3. The experimental data from the tensile test of specimen DB #U1-1

In Figure 8, we see that the slope of tension behaviour curve changed when the average tensile strain was approximately 0.15%. Crack width was almost the same ($w=0.04$ mm) within the strain range between 0.50‰ and 2.0‰, which led to the stabilized cracking stage happening within this strain range.

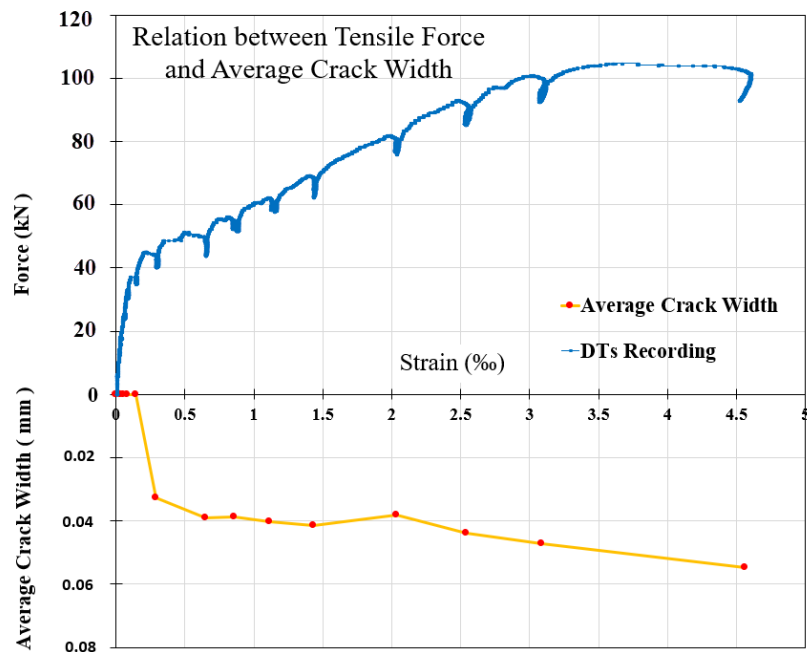
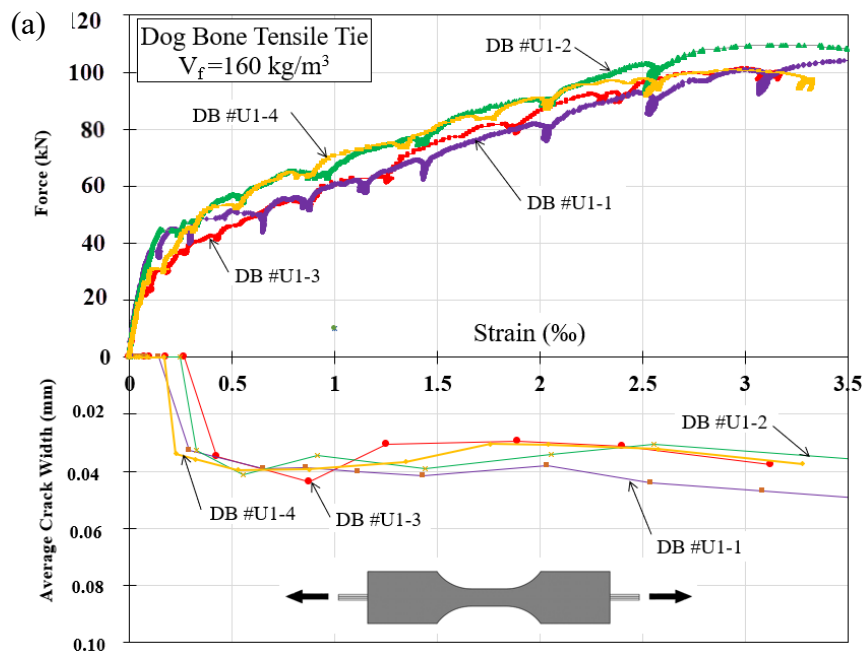


Figure 8. The force-strain and crack width-strain relations of specimen DB #U1-1

Figures 9a and 9b illustrate the results obtained for all the specimens from the two employed UHPFRC types. It is important to mention that specimen DB #U2-4, with concrete type U2 ($V_f=80 \text{ kg/m}^3$), failed due to an improper friction between the jaw dents and the rebar surface. According to these figures, the first cracks happened before the 0.5% average tensile strain for both UHPFRC types (U1 and U2). The crack width value for specimens with UHPFRC type U1 at a strain level above 0.5% was almost constant (0.040 mm), while for the specimens with UHPFRC type U2, the crack width at the strain level between 0.5 and 1.0% was almost 0.070 mm and almost 0.055 mm for the strain level higher than 1.0%. By considering the same mixture composition for UHPFRC types U1 and U2, the difference between crack width could be caused by the difference in the fibre volume contents for each UHPFRC type. Regarding the SLS requirements (crack width controlling) for UHPFRC and durability issues, the R-UHPFRC tensile elements with the 2. vol% fibre content behaved better than the tensile R-UHPFRC elements with the 1. vol% fibre content. For the UHPFRC U1 type, crack width was narrower than type U2 and its value remained approximately constant up to the high tensile strain rate.



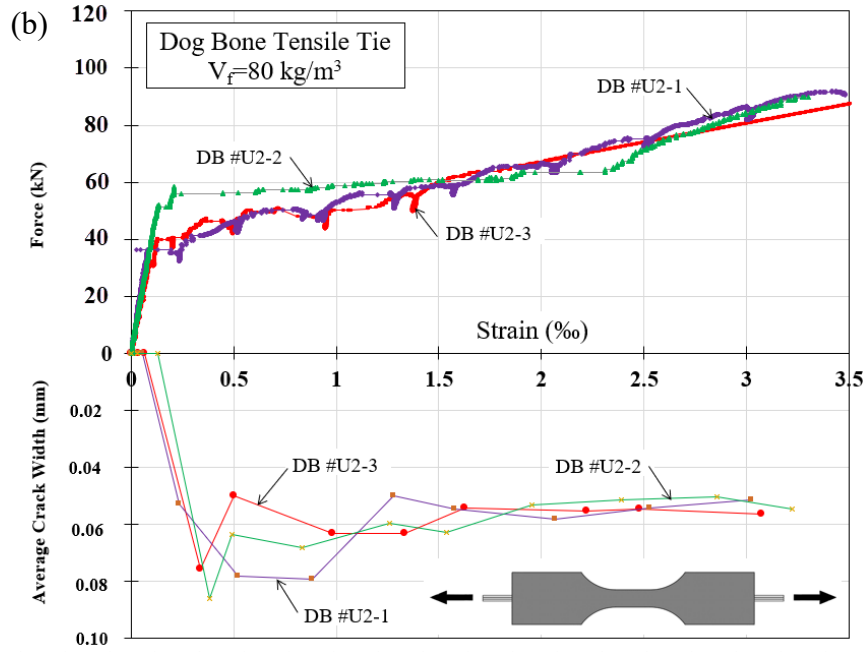


Figure 9. Force-strain and crack width-strain curves of the dog bone-shaped R-UHPFRC ties

(a) $V_f = 160 \text{ kg/m}^3$, (b) $V_f = 80 \text{ kg/m}^3$






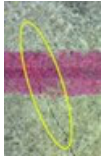

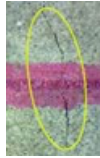
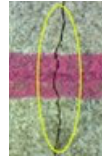

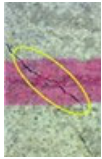
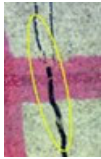





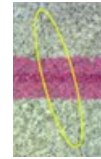

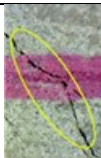





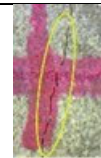
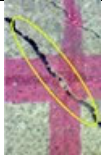
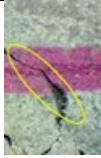
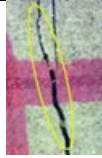
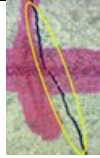
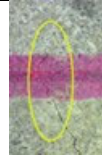
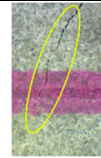

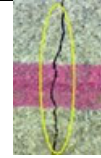

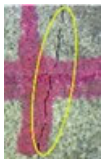
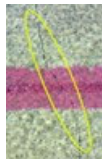

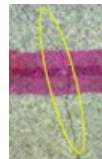
Shrinkage is an essential effect to be considered in R-UHPFRC, inducing significant tensile strains in the concrete matrix, and therefore, modifying the general tensile behaviour of the R-UHPFRC tie elements. French code NF P 18-710 [17] provides an indicative value of $550 \mu\text{m/m}$ for UHPFRC shrinkage. A primary study about this effect on the behaviour of R-UHPFRC ties with the same UHPFRC employed herein has been performed by the authors [34], but an in-depth study is needed to consider all the effective UHPFRC shrinkage factors.

5.2. Maximum crack width

The maximum crack width was obtained by reviewing the recorded video and monitoring all cracks. Table 4 provides a series of formed crack images on the central axial line (L1) of specimen DB #U1-1 as a sample (in this study) to understand the maximum crack width calculation, as well as the crack formation process. Table 4 indicates the average tensile applied force value (F_{avg}) of the initial and final recording processes, where (w_{max}) is the maximum value of the detected crack width on line L1, (n) is the number of cracks on line L1, (w_{avg}) is the average crack width calculated by dividing the tensile elongation by the number of cracks and (ϵ_t) is the average tensile strain value of the initial and final recording video process.

According to the images obtained from specimen DB #U1-1 test, i.e. for force stage N10, the cracks that formed along the specimen had different width values. Therefore due to crack width

variation, the difference between the average crack width value ($w_{avg} = 0.0321$ mm) and the maximum value ($w_{max} = 0.1000$ mm) was significant. The diagrams presented in Fig. 10 provide the calculated average and maximum crack width values for the 10 load stages analysed.

Test data	Captured images of the cracks							
<u>N5</u> n = 4 $F_{avg} = 41.5$ kN $w_{max} = 0.0440$ mm $w_{avg} = 0.0218$ mm $\epsilon_t = 0.291\%$					-	-	-	-
<u>N6</u> n = 6 $F_{avg} = 46.9$ kN $w_{max} = 0.0500$ mm $w_{avg} = 0.0326$ mm $\epsilon_t = 0.651\%$							-	-
<u>N7</u> n = 8 $F_{avg} = 53.4$ kN $w_{max} = 0.0750$ mm $w_{avg} = 0.0322$ mm $\epsilon_t = 0.859\%$								
<u>N8</u> n = 10 $F_{avg} = 60.3$ kN $w_{max} = 0.0750$ mm $w_{avg} = 0.0335$ mm $\epsilon_t = 1.115\%$								
<u>N9</u> n = 13 $F_{avg} = 63.9$ kN $w_{max} = 0.0620$ mm $w_{avg} = 0.0330$ mm $\epsilon_t = 1.43\%$								
						-	-	-

N10

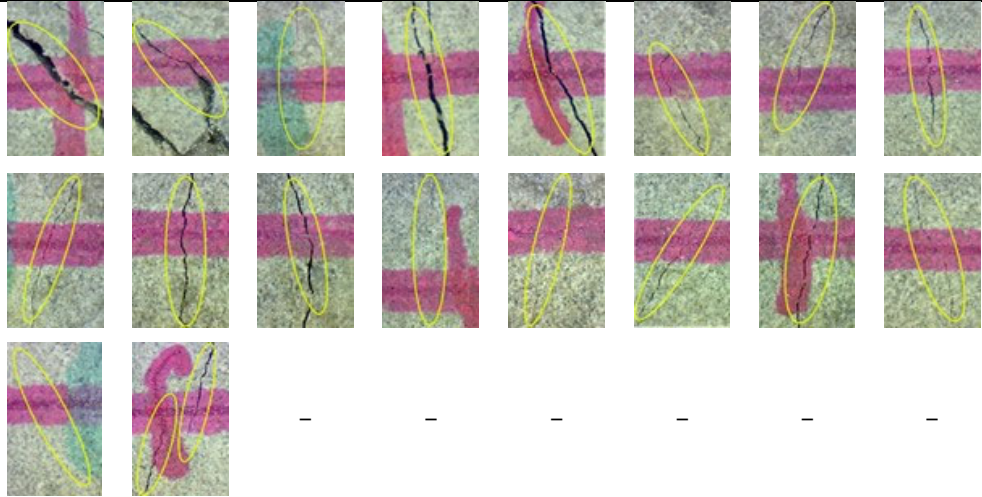
n = 19

$F_{avg} = 78.8 \text{ kN}$

$w_{max} = 0.1000 \text{ mm}$

$w_{avg} = 0.0321 \text{ mm}$

$\epsilon_t = 2.035\%$



N11

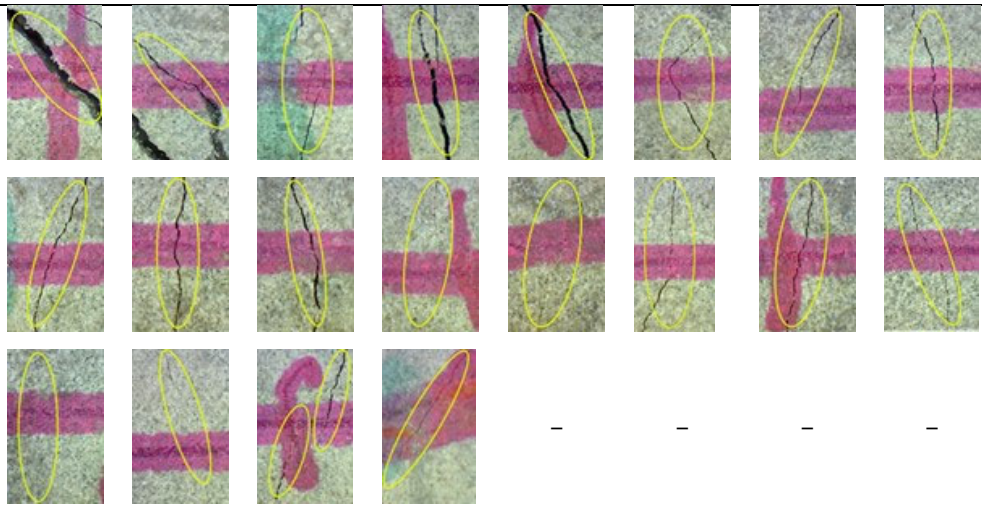
n = 21

$F_{avg} = 87.9 \text{ kN}$

$w_{max} = 0.1870 \text{ mm}$

$w_{avg} = 0.0363 \text{ mm}$

$\epsilon_t = 2.540\%$



N12

n = 23

$F_{avg} = 93.2 \text{ kN}$

$w_{max} = 0.3120 \text{ mm}$

$w_{avg} = 0.0402 \text{ mm}$

$\epsilon_t = 3.085\%$

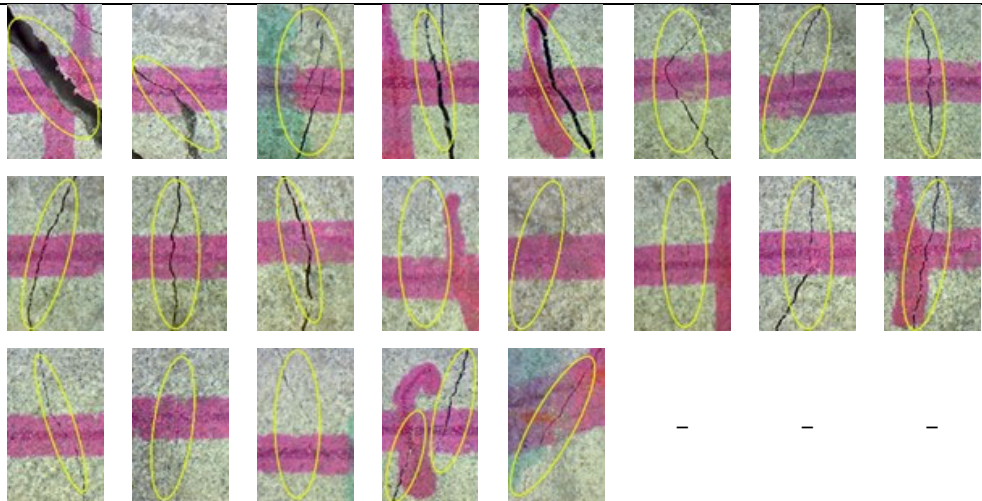
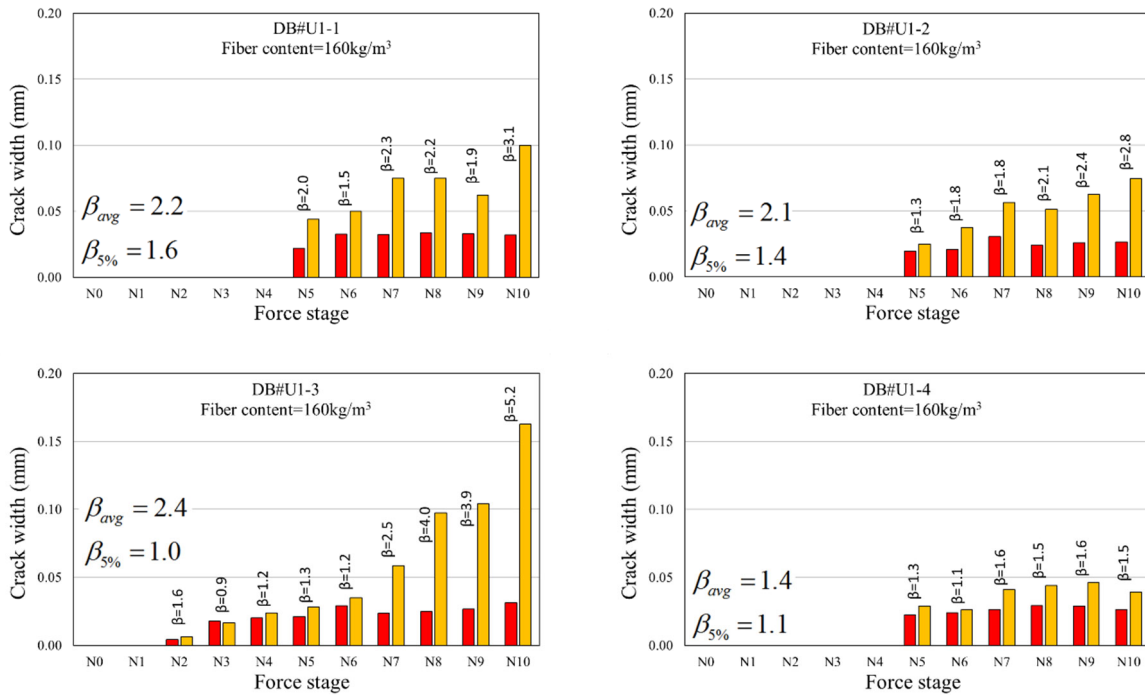


Table 4. Cracks captured during the tensile test of specimen DB #U1-1 on the central axial line (L1).

Specimens with UHPFRC type U1 ($V_F=160\text{ kg/m}^3$)



Specimens with UHPFRC type U2 ($V_F=80\text{ kg/m}^3$)

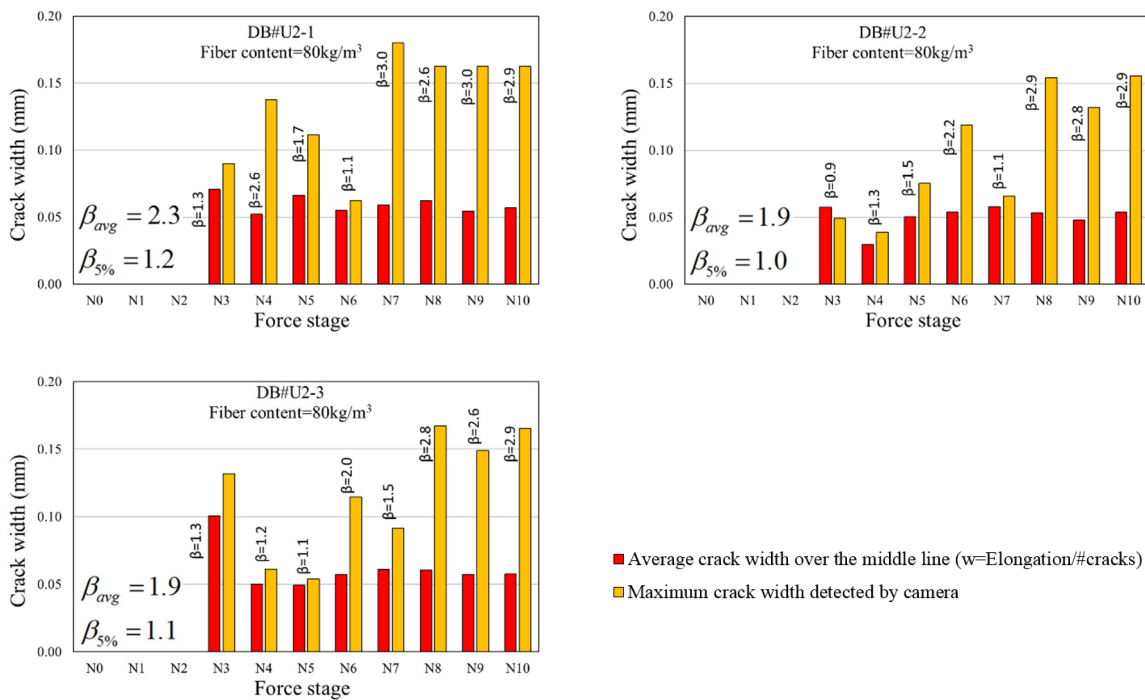


Figure 10. Comparing the maximum crack width to the average crack width values for the R-UHPFRC tie elements with UHPFRC types U1 and U2

As previously explained in Section 1, under service loads, (β) is defined as the factor that relates the ratio between the characteristic crack width (or the maximum crack width) and the average crack width values ($\beta = w_k / w_m$). This (β) factor was calculated for each applied force stage, along with its value for each stage (Fig. 10). Obviously, the maximum crack width values at high applied tensile force values (Stages N9 and N10) and at the high tensile strain rate (between 2.0‰ and 3.5‰) could be more than 2.8-fold the average crack width values (the average value β for two last force stages for all specimens) for both UHPFRC types U1 and U2. The mean β_{avg} values for the tensile elements were 2.02 and 2.03 for UHPFRC type U1 and type U2, respectively. In experimental terms, it can be assumed that the maximum crack width (w_k) can be calculated by multiplying the average crack width ($w_m = \text{elongation}/\text{number of cracks}$) by β (approximately $\beta = 2.0$) for both UHPFRC types. It should be noted that the $\beta = 2.0$ value was obtained as the average of the values from the low to high tensile strain rates (up to 3.5‰ in some cases). In the SLS design of the concrete elements, the characteristic crack width should be calculated under service loads so that tensile strain would be far less under SLS conditions. French code NF P 18-710 [17] provides the maximum crack width limitations for the SLS design of the UHPFRC structure elements under service conditions. To meet the serviceability requirement, the crack widths of the elements under service loads should go below these values. By comparing the obtained experimental maximum crack width values (see the diagrams in Fig. 10) to the limit values of NF P 18-710 in Table 7.201 [17], almost all the experimental maximum crack widths of R-UHPFRC type U1 (fibre content=160 kg/m³) were less than 0.10 mm. This means that the R-UHPFRC type U1 met the crack width limitation for all the exposure classes. However, the maximum experimental crack width for UHPFRC type U2 (fibre content=80 kg/m³) obtained values that came close to 0.15 mm, which does not meet the SLS requirement for exposure classes XD1, XD2, XD3, XS1, XS2, and XS3 (corrosion induced by chlorides and seawater).

5.3. Crack number

Cracking behaviour can be evaluated by the number of cracks at a given average tensile strain. The cracking data were obtained by counting the number of cracks at three tensile strain levels to evaluate and compare the cracking phenomenon for the two used UHPFRC types. The measured number of cracks for the tensile strain values of 1.0‰, 2.0‰ and 3.0‰ are found in Figure 11.

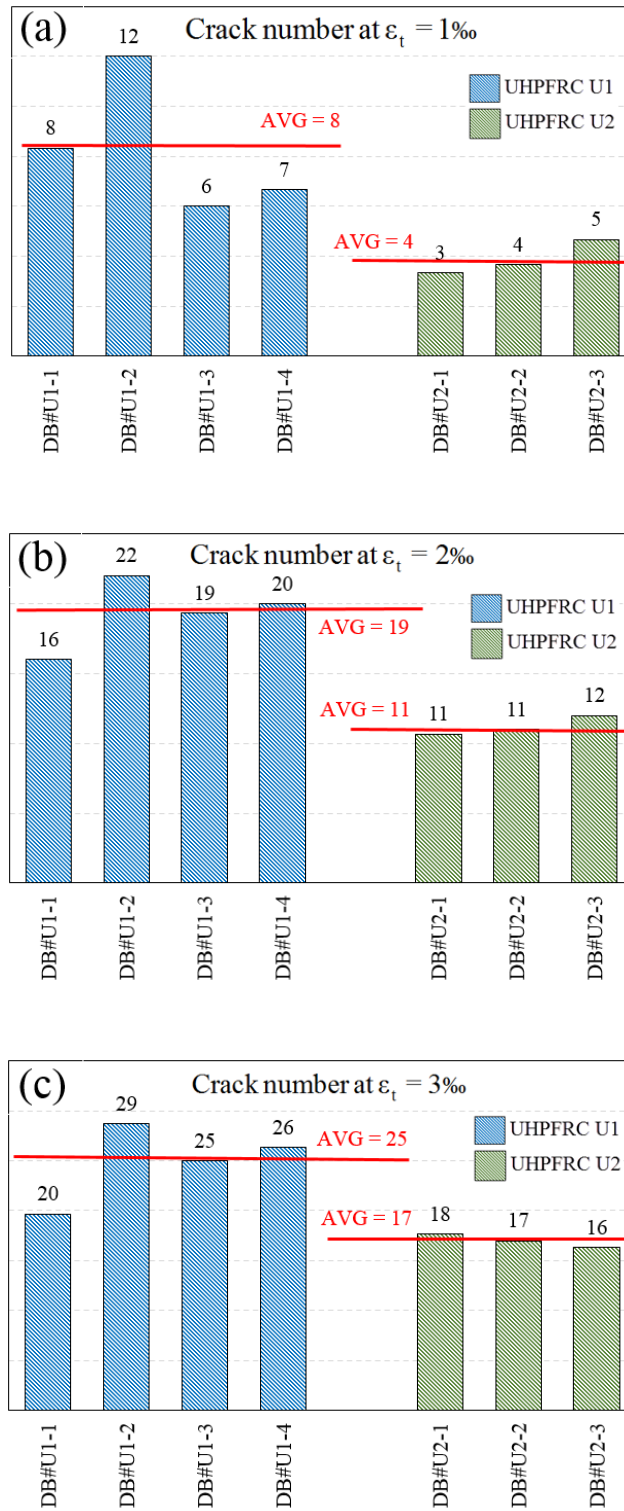
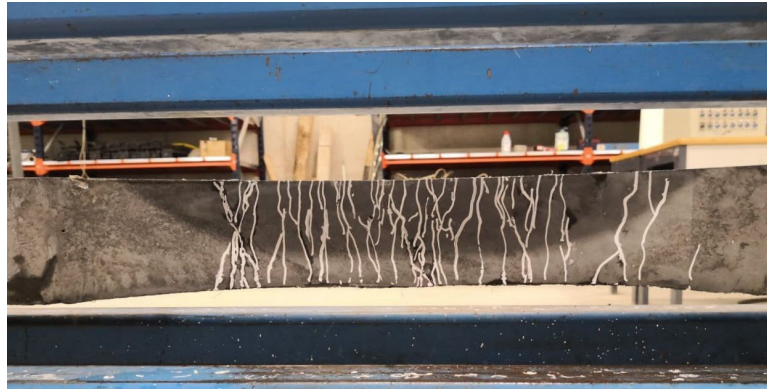


Figure 11. Comparing the crack number values for tensile strain values: (a) 1.0%, (b) 2.0% and (c) 3.0%.

Fibre content very clear influenced the specimens with two different fibre volume contents (U1 with $V_f=160 \text{ kg/m}^3$ and U2 with $V_f=80 \text{ kg/m}^3$), especially considering that all the specimens had an identical UHPFRC matrix, rebar diameter and cross-section dimensions. The average value of the number of cracks obtained for the specimens with UHPFRC type U1 increased from 8 to 25 (almost 3-fold) simply by increasing tensile strain from 1.0% to 3.0%. For the

specimens with UHPFRC type U2, the number of the cracks rose from 3 to 17 (almost 6-fold). Hence crack spacing decreased with increasingly applied tensile strain. From the photographs in Figure 12, the crack spacing for the specimens with UHPFRC type U1 is narrower than it is for UHPFRC type U2, and it displays better microcrack propagation behaviour.

(a)



(b)

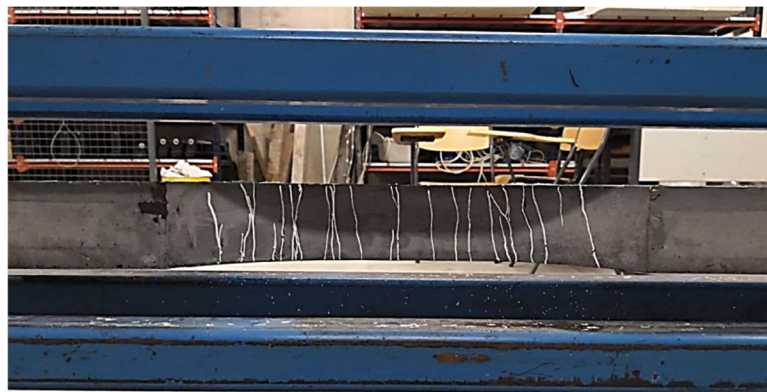


Figure 12. The crack pattern obtained at the 3.5‰ tensile strain level, a) specimen DB #U1-1 with $V_f = 160 \text{ kg/m}^3$, b) specimen DB #U2-1 with $V_f = 80 \text{ kg/m}^3$.

From these observations, we note that the number of cracks and the average crack spacing of the UHPFRC tensile elements were influenced by fibre content.

5.4. Developing a fragility curve for the cracking data

A probability distribution is a statistical function that describes all the possible values and likelihoods that a random variable can take within a given range [41]. An alternative description of distribution is given by the cumulative distribution function (CDF), which is the probability of the value of the variable being less than or equaling x [42].

$$F(x) = P[X \leq x] = \alpha \quad (3)$$

The CDF is the area according to the probability density function from $-\infty$ to x . For continuous distribution, it can be expressed mathematically as Eq. 4:

$$F(x) = P[-\infty < X \leq x] = \int_{-\infty}^x f(x) dx \quad (4)$$

For discrete distribution, the CDF can be expressed as Eq.5:

$$F(x) = P[X \leq x] = \sum_{i=0}^x f(i) \quad (5)$$

On probability curves, the horizontal axis is the allowable domain for the given probability function. As the vertical axis is a probability, it must fall between zero and one.

In the present research, we used the Rice probability density function (Eq. 6) and the corresponding CDF (Eq. 7).

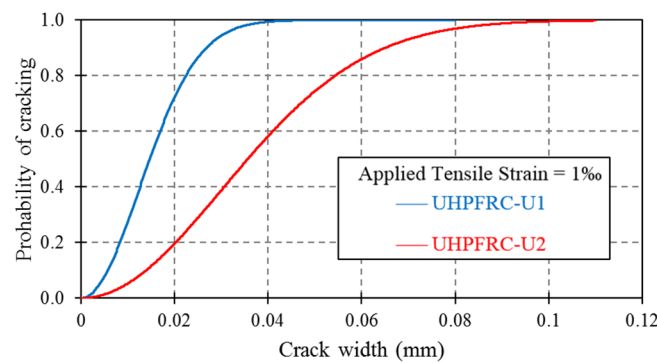
$$f(x) = \frac{x}{\sigma^2} \exp\left(\frac{-(x^2 + \nu^2)}{2\sigma^2}\right) I_0\left(\frac{x\nu}{\sigma^2}\right) \quad (6)$$

$$f(x) = 1 - Q_1\left(\frac{\nu}{\sigma}, \frac{x}{\sigma}\right) \quad (7)$$

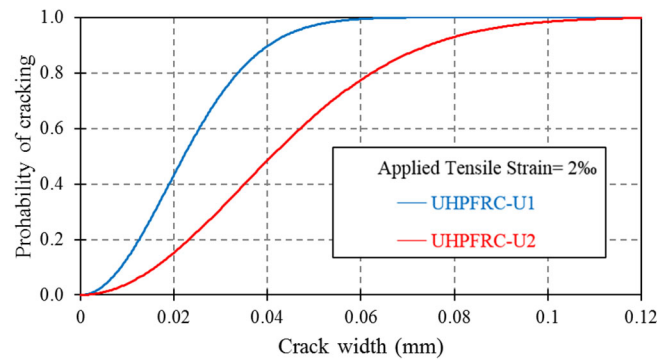
where σ and ν are continuous parameters, I_0 is the modified Bessel function of the first kind with order zero, and Q_1 is the Marcum Q-function.

A fragility function (or a fragility curve) represents the CDF of an asset's capacity to resist an undesirable limit state [43]. We applied this analysis method to present the probability of exceeding crack width with a specific tensile strain for UHPFRC types U1 and U2. Fragility curves were calculated based on all the crack widths detected for all the specimens at the applied tensile strains of 1.0‰, 2.0‰ and 3.0‰ (see Fig. 13).

(a)



(b)



(c)

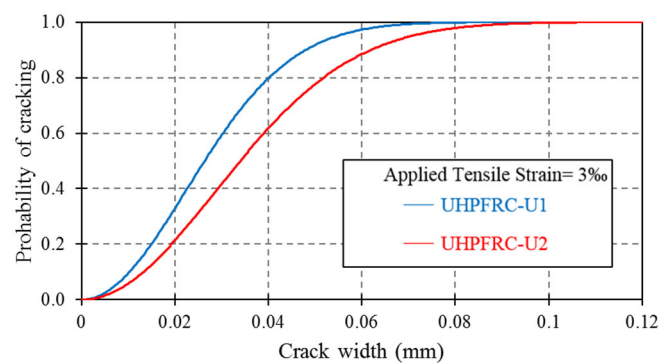


Figure 13. Fragility curves based on the cracking data obtained for the specimens with UHPFRC U1 and U2: tensile strain level (a) 1.0‰; (b) 2.0‰; (c) 3.0‰.

At all different applied tensile strain levels, the probability curve of UHPFRC type U1 was placed on top of the UHPFRC type U2 probability curve. This means that for the specific probability level, the UHPFRC type U2 had a wider crack width. For a high tensile strain rate (see Fig. 13.c), the probability curve of the two UHPFRC came closer to one another and the difference between them was smaller. This behaviour can be explained by the fibre pull-out mechanism that happens at the high tensile strain rate. At these rates of tensile strains, almost all the fibres were pulled out from the concrete matrix and, therefore, tensile stresses were mostly carried out by steel rebars. As the steel rebar diameter was the same for the two considered UHPFRC concretes, both curves were close together. Hence, for the UHPFRC elements with a high steel reinforcement rate, the steel fibre efficiency in the ultimate limit state was poor.

In order to better understand the difference between the fragility curve behaviour of UHPFRC types U1 and U2, the crack widths corresponding to the 5%, 50%, and 95% probability levels are presented in Table 5. These values represent the lower and higher characteristic values of the results.

UHPFRC type	Lower characteristic value (5% of the results)	Mean value (50% of the results)	Higher characteristic value (95% of the results)	$\left(\beta = \frac{w_{95\%}}{w_{50\%}} \right)$
1 ‰				
U1	0.004	0.015	0.031	2.07
U2	0.010	0.036	0.074	2.08
2 ‰				
U1	0.006	0.022	0.046	2.08
U2	0.011	0.041	0.085	2.09
3 ‰				
U1	0.007	0.026	0.055	2.09
U2	0.009	0.034	0.071	2.08

Table 5. Crack width corresponding to the probability 0.05, 0.50 and 0.95 values for UHPFRC U1 and U2 (units: in mm)

By increasing the tensile strain rate, the crack width values rose. For all cases, UHPFRC type U2 obtained higher crack width values. In serviceability behaviour terms, at the probability level of 0.95 (see Table 5), crack width was narrower than the limit crack width limitation value defined by French code NF P 18-710 [17] for UHPFRC elements (0.1 mm, the lowest value for R-UHPFRC members). Neither UHPFRC type exceeded this crack width limitation despite the fact that the average strains surpassed the level of the reinforcement yielding. The β value was calculated by dividing the maximum value ($w_{95\%}$) by the mean value ($w_{50\%}$). The β values obtained by this method can be considered reliable and accurate enough to relate the maximum to the average crack width values.

6. Conclusions

An experimental program based on direct tensile tests was performed to study the cracking behaviour of R-UHPFRC by also comparing the maximum crack widths to average values. In this study, two UHPFRC types with different fibre volume contents were used and the main following conclusions were drawn:

- For both the R-UHPFRC tensile elements with UHPFRC types U1 ($V_f = 2\%$) and U2 ($V_f = 1\%$), the first detected crack occurred at a lower tensile strain level than 0.5%. Average crack width after the first cracking for the R-UHPFRC ties with UHPFRC type U1 was almost constant with a value of about 0.04 mm, and one of about 0.07 mm for type U2

- The maximum crack width (obtained by a microscope camera that detected all cracks) can be more than double the average crack width, and the β factor can be accepted as two.
- As expected, R-UHPFRC type U1 generally demonstrated better cracking behaviour than R-UHPFRC type U2. At the high applied tensile strain level (up to 3.5‰ in this study), the maximum crack width obtained values up to 0.1 mm, which means that this UHPFRC type can meet the crack width limitation for all exposure classes
- The characteristic crack width value obtained from the fragility curves corresponding to the probability level of 0.95 under SLS conditions was narrower than the crack width limitation by French code NF P 18-710 (0.1 mm, the lowest value for R-UHPFRC members). This result leads to the conclusion that both reinforced UHPFRC types can meet the serviceability crack width limitation, thanks to the rebars and fibres synergy.

Acknowledgments

This study forms part of Project BIA2016-78460-C3-1-R, supported by the Ministry of Economy and Competitiveness of Spain.

References

1. Boschmann Käthler, A., et al., *Effect of cracks on chlorideinduced corrosion of steel in concrete-a review: Etatsprogrammet Varige konstruksjoner 2012-2015*. 2017.
2. El-Joukhadar, N. and S. Pantazopoulou, *Effectiveness of UHPFRC cover in delaying bar corrosion*. Construction and Building Materials, 2021. **269**: p. 121288.
3. Wu, C., J. Li, and Y. Su, *Development of ultra-high performance concrete against blasts: From materials to structures*. 2018: Woodhead Publishing.
4. Schmidt, M. and E. Fehling, *Ultra-high-performance concrete: research, development and application in Europe*. ACI Special publication, 2005. **228**: p. 51-78.
5. Rahman, S., T. Molyneaux, and I. Patnaikuni, *Ultra high performance concrete: recent applications and research*. Australian journal of civil engineering, 2005. **2**(1): p. 13-20.
6. Shin, W. and D.-Y. Yoo, *Influence of steel fibers corroded through multiple microcracks on the tensile behavior of ultra-high-performance concrete*. Construction and Building Materials, 2020. **259**: p. 120428.
7. fib, *Model Code 2010-First complete draft-Volume 2: Model Code*. 2010, fib Fédération internationale du béton.
8. Eurocode2:, *Design of concrete structures: Part 1-1: General rules and rules for buildings*. 2004: British Standards Institution.
9. Committee, A.C.I., et al., *Building code requirements for structural concrete (ACI 318-19) : an ACI standard ; Commentary on building code requirements for structural concrete (ACI 318R-19)*. 2019.
10. Sunaga, D., K. Namiki, and T. Kanakubo, *Crack width evaluation of fiber-reinforced cementitious composite considering interaction between deformed steel rebar*. Construction and Building Materials, 2020. **261**: p. 119968.
11. Borosnyói, A. and G.L. Balázs, *Models for flexural cracking in concrete: the state of the art*. Structural Concrete, 2005. **6**(2): p. 53-62.
12. Bruggeling, A.S.G., *Structural concrete: theory and its application*. 1991.
13. Rizkalla, S. and L. Hwang, *Crack prediction for members in uniaxial tension*. in *Journal Proceedings*. 1984.

14. Broms, B.B. and L.A. Lutz. *Effects of arrangement of reinforcement on crack width and spacing of reinforced concrete members*. in *Journal Proceedings*. 1965.
15. CPH., "Instrucción de Hormigón Estructural EHE-08." *Comisión Permanente Del Hormigón. Ministerio De Fomento*. 2008: Madrid (Spain).
16. CNR-DT 203. (2006). *Guide for the Design and Construction of Concrete Structures Reinforced with Fiber-Reinforced Polymer Bars.*" *Advisory Committee on Technical Recommendations for Construction*.
17. NF P 18-710, *Complément national à l'Eurocode 2 — Calcul des structures en béton : règles spécifiques pour les Bétons Fibrés à Ultra-Hautes Performances (BFUP)*. AFNOR, France, 2016.
18. CEB-FIP, M., 90, *Design of concrete structures. CEB-FIP Model Code 1990*. British Standard Institution, London, 1993.
19. Vandewalle, L., et al., *Rilem TC 162-TDF: Test and design methods for steel fibre reinforced concrete: Uni-axial tension test for steel fibre reinforced concrete*. *Materials and Structures/Materiaux et Constructions*, 2001. **34**(235): p. 3-6.
20. Fehling, E., et al., *Ultra-high performance concrete UHPC: Fundamentals, design, examples*. 2015: John Wiley & Sons.
21. Leutbecher, T. and E. Fehling, *Crack width control for combined reinforcement of rebars and fibers exemplified by ultra-high-performance concrete*. fib task group, 2008. **8**: p. 1-28.
22. Leutbecher, T. and E. Fehling, *Design for serviceability of ultra high performance concrete structures*, in *High Performance Fiber Reinforced Cement Composites 6*. 2012, Springer. p. 445-452.
23. Leutbecher, T. and E. Fehling, *Rissbildung und Zugtragverhalten von mit Fasern verstärktem Stahlbeton am Beispiel ultrahochfesten Betons: Teil 1: Rissmechanische Zusammenhänge*. *Beton-und Stahlbetonbau*, 2009. **104**(6): p. 357-367.
24. Leutbecher, T. and E. Fehling, *Rissbildung und Zugtragverhalten von mit Fasern verstärktem Stahlbeton am Beispiel ultrahochfesten Betons—Teil 2: Experimentelle Untersuchungen und Anwendungsbeispiele*. *Beton-und Stahlbetonbau 104 (2009), Issue 7*, p. 406–415.
25. Le Hoang, A. and E. Fehling, *Influence of steel fiber content and aspect ratio on the uniaxial tensile and compressive behavior of ultra high performance concrete*. *Construction and Building Materials*, 2017. **153**: p. 790-806.
26. Committee, J.C., *Recommendations for design and construction of high performance fiber reinforced cement composites with multiple fine cracks*. Japan Society of Civil Engineers, Tokyo, Japan, 2008.
27. Cahier Technique, S., *Béton fibré ultra-performant (BFUP)-Matériaux, dimensionnement et exécution*. *Projet*, 2014.
28. Khorami, M., J. Navarro-Gregori, and P. Serna, *Experimental methodology on the serviceability behaviour of reinforced ultra-high performance fibre reinforced concrete tensile elements*. *Strain*: p. e12361.
29. Khorami, M., et al. *A testing method for studying the serviceability behavior of reinforced UHPFRC tensile ties*. in *IOP Conference Series: Materials Science and Engineering*. 2019. IOP Publishing.
30. Albitar, M., M.M. Ali, and P. Visintin, *Evaluation of tension-stiffening, crack spacing and crack width of geopolymers concretes*. *Construction and Building Materials*, 2018. **160**: p. 408-414.
31. JSCE, C.C., *Recommendations for design and construction of high performance fiber reinforced cement composites with multiple fine cracks*. Japan Society of Civil Engineers, Tokyo, Japan, 2008.
32. 190-85, A., *Method of test for tensile strength of hydraulic cement mortars*. 1985, ASTM Philadelphia PA.
33. Yokota, H., K. Rokugo, and N. Sakata. *JSCE recommendations for design and construction of high performance fiber reinforced cement composite with multiple fine cracks*. in *High Performance Fiber Reinforced Cement Composites*. 2008.
34. Khorami, M., J. Navarro-Gregori, and P. Serna, *Tensile behaviour of reinforced UHPFRC elements under serviceability conditions*. *Materials and Structures*, 2021. **54**(1): p. 43.
35. Máca, P., R. Sovják, and P. Konvalinka, *Mix design of UHPFRC and its response to projectile impact*. *International Journal of Impact Engineering*, 2014. **63**: p. 158-163.
36. Shi, C., et al., *A review on ultra high performance concrete: Part I. Raw materials and mixture design*. *Construction and Building Materials*, 2015. **101**: p. 741-751.
37. López, J.Á., et al., *An inverse analysis method based on deflection to curvature transformation to determine the tensile properties of UHPFRC*. *Materials and Structures*, 2015. **48**(11): p. 3703-3718.
38. López Martínez, J.A., *Characterisation of The Tensile Behaviour of UHPFRC by Means of Four-Point Bending Tests*. 2017.

39. Mezquida-Alcaraz, E.J., J. Navarro-Gregori, and P. Serna-Ros, *Direct procedure to characterize the tensile constitutive behavior of strain-softening and strain-hardening UHPFRC*. *Cement and Concrete Composites*. **115**: p. 103854.
40. Lopez, J.A., et al., *First ultra-high-performance fibre-reinforced concrete footbridge in Spain: Design and construction*. *Structural Engineering International*, 2014. **24**(1): p. 101-104.
41. Ash, R.B., *Basic probability theory*. 2008: Courier Corporation.
42. Dekking, F.M., et al., *A Modern Introduction to Probability and Statistics: Understanding why and how*. 2005: Springer Science & Business Media.
43. Porter, K., *A beginner's guide to fragility, vulnerability, and risk*. *Encyclopedia of earthquake engineering*, 2015. **2015**: p. 235-260.